

Supplement of Atmos. Chem. Phys., 16, 12649–12666, 2016
<http://www.atmos-chem-phys.net/16/12649/2016/>
doi:10.5194/acp-16-12649-2016-supplement
© Author(s) 2016. CC Attribution 3.0 License.



Atmospheric
Chemistry
and Physics
Open Access
EGU

Supplement of

Inverse modeling of pan-Arctic methane emissions at high spatial resolution: what can we learn from assimilating satellite retrievals and using different process-based wetland and lake biogeochemical models?

Zeli Tan et al.

Correspondence to: Qianlai Zhuang (qzhuang@purdue.edu)

The copyright of individual parts of the supplement might differ from the CC-BY 3.0 licence.

S1. Methods and Results

In the text S1, the steps to construct optimal initial conditions for global and nested grid inversions are described. We also describe the steps to construct an optimal GEOS-Chem CH₄ field for SCIAMACHY bias correction purpose and the comparison between our estimates and previous inversion studies in the global scale.

To start global and nested-grid inversions, the initial CH₄ field of the GEOS-Chem model needs to be optimized to minimize its error. As our focus is in the period of 2004–2005, to speed up the whole process, we only ran one inversion from 1993 to 2003 using the LPJ-WSL scenario and NOAA/ESRL measurements. The main purpose of this inversion is to construct initial CH₄ field in 2004. As presented in Fig. S2, without optimization, the LPJ-WSL scenario gives the best fit of the GEOS-Chem modeled CH₄ to the GLOBALVIEW-CH₄ data (GLOBALVIEW-CH₄, 2009). During the 1993–2003 inversion, GEOS-Chem was driven by GEOS-4 meteorological (met) data from NASA's Global Modeling Assimilation Office (GMAO). Relative to GEOS-5, the GEOS-4 met data has the same horizontal resolutions but less vertical hybrid sigma-pressure levels (55 vertical levels).

To construct optimal atmospheric CH₄ fields for the bias correction of SCIAMACHY retrievals at the global scale, we ran a global inversion during 2004–2005 using the LPJ-WSL wetland emission scenario and NOAA/ESRL measurements. In this inversion, the GEOS-Chem model was driven by the GEOS-5 met data. The global inversions of different scenarios that assimilated both surface measurements and satellite retrievals were then run in two sequential time windows: 2004/01–2004/12 and 2005/01–2005/12. Only the inversions in the second time window are for analysis and the first time window is designed to minimize the impacts of the

transition from GEOS-4 to GEOS-5 and from the LPJ-WSL scenario to other scenarios. In the above inversions, we included surface measurements from pan-Arctic sites but excluded satellite retrievals out of 50°S–50°N. The global inversions during 2005 also provided initial conditions and time-dependent boundary conditions for the nested grid simulations of the adjoint model. Following Turner et al. (2015), we did not optimize boundary conditions in the nested-grid inversions as did in Wecht et al. (2014). The nested grid inversions of the pan-Arctic were run at $1/2^\circ \times 2/3^\circ$ resolution from July 1, 2005 to Oct 1, 2005.

Specific humidity for bias correction was retrieved from the European Centre for Medium-Range Weather Forecasts (ECMWF)'s ERA-20C reanalysis product (<http://apps.ecmwf.int/datasets/data/era20c-daily>), averaged by the column between the surface and 3 km altitude (Houweling et al., 2014). The air mass factor and coordinates of satellite CH₄ retrievals have been included in the SCIAMACHY IMAP v6.0. For global-scale bias correction, we first optimized the GEOS-Chem 4-D CH₄ mixing ratios using only surface measurements and then sampled the modeled XCH₄ at the coordinates and time of SCIAMACHY retrievals and with local averaging kernels applied. Following Bergamaschi et al. (2009) and Houweling et al. (2014), only satellite retrievals between 50°S and 50°N were utilized. The XCH₄ differences between SCIAMACHY and GEOS-Chem are shown in Fig. S3a. A regression relationship was then built to represent the satellite system bias by proxy factors. Turner et al. (2015) suggested that it is more likely that grid squares residual standard deviation (RSD) in excess of 20 ppb are dominated by model bias in prior emissions. Thus, we excluded such grid squares in regressions. And satellite retrievals with low precisions (the ratio of retrieval precision error to retrieval is larger than 3%) were also removed from analysis. Following Houweling et al. (2014), we did not optimize bias correction functions in the inversion cycle in the concern that this process could

cause bias correction to incorrectly account for the uncertainties caused by unaccounted model errors or even the uncertain sources and sinks. As shown in Fig. S3d, bias correction reduced model-satellite differences greatly in tropical areas of America, Africa and South Asia and also reduced the differences in Australia and some areas of the United States. And the agreement between GEOS-Chem and SCIAMACHY is also improved at the global scale (Fig. S3c). However, the model-data agreement is deteriorated in East Asia. It could be caused by the overestimate of anthropogenic CH₄ emissions from China in the EDGAR dataset (Peng et al., 2016).

The results of the global inversions are presented in Table 2 and Fig. S4. There have been many studies that assimilated surface measurements and/or satellite retrievals into a CTM inverse model to constrain global CH₄ emissions, see Kirschke et al. (2013) for review. For instance, using the same observations suite, Bergamaschi et al. (2009) estimated that in 2004, CH₄ emissions in global, tropical (30°S–30°N), northern extratropical (30°N–90°N) and southern extratropical (90°S–30°S) zonal areas were 506.7 Tg CH₄ yr⁻¹, 323.5 Tg CH₄ yr⁻¹, 172.8 Tg CH₄ yr⁻¹ and 10.4 Tg CH₄ yr⁻¹, respectively. These large-scale estimates are consistent with our calculations: 284.5–319.6 Tg CH₄ yr⁻¹ (tropical), 165.3–206.6 Tg CH₄ yr⁻¹ (northern extratropical) and 10.0–13.9 Tg CH₄ yr⁻¹ (southern extratropical). This agreement could imply that the GEOS-Chem adjoint and TM5-4DVAR are consistent in the atmospheric transport, chemistry and inverse modeling methods. In contrast to Bergamaschi et al. (2009), our inversions allocate more emissions to extratropical regions. As a result, the tropical total (SATr + NAF + SAF + TrA) of the six inversions is in the range of 114.1–169.7 Tg CH₄ yr⁻¹, which is much lower than their estimate of 203.2 Tg CH₄ yr⁻¹. The likely reason for this discrepancy is that we did not optimize bias correction functions in the inversion cycle. Our posterior wetland CH₄ emissions estimated

in the Bern, CLM4Me, SDGVM and WSL scenarios are close to the estimate of 161 Tg CH₄ yr⁻¹ for 2003–2007 in Bloom et al. (2010). The latter was based on CH₄ and gravity spaceborne data to constrain large-scale methanogenesis. Our estimates are also close to the inferred wetland CH₄ emissions (175±33 Tg CH₄ yr⁻¹) by Kirschke et al. (2013). By using artificial neural networks, Zhu et al. (2013) estimated that from 1990 to 2009, annual wetland CH₄ emissions from northern high latitudes (> 45°N) were in the range of 44.0–53.7 Tg CH₄ yr⁻¹, agreeing with the estimates of the Bern, CLM4Me and SDGVM scenarios.

Fig. S4a shows that CH₄ fluxes are the highest in the Amazon, China, Southeast Asia, North America and Europe where there are either a large area of wetlands and rice paddies or advanced coal and oil industries or both. Our results indicate that the Eurasian temperate zone, including China, North America and Europe, emitted much more CH₄ than any other geographic zones (Table 2), implying the dominance of anthropogenic sources in the global CH₄ inventory. As presented in Fig. S4c, our inverse modeling reduced the CH₄ emissions from China, the Amazon basin and the Eurasian boreal region (scale factor < 1) but increased the emissions in Europe and Southeast Asia (scale factor > 1) relative to the prior.

Fig. S6 shows the difference between the modeled and observed CH₄ mixing ratios at NOAA ship board sampling stations and aircraft vertical profile sites under different wetland scenarios before and after the global scale inversions. For most scenarios, inversion improves the representation of CH₄ mixing ratios in GEOS-Chem at both marine and inland boundary layers and free troposphere. For example, the BERN scenario inversion reduced the bias by about 18 ppb for ship stations and about 6 ppb for aircraft sites. Also the DLEM scenario inversion reduced the bias by about 20 ppb for ship stations and about 19 ppb for aircraft sites. For the CLM4Me and SDGVM scenarios with low prior biases, the inversions did not improve the

performance. This could be caused by the errors introduced by the inversion process itself. For example, as the optimization is designed to address total emissions, the representation of diurnal variability in GEOS-Chem could be made worse during inversion.

Table S1. NOAA/ESRL stations used in the inversion.

Station ID	Latitude	Longitude	Altitude [m]	Station Name
ALT	82.45	-62.52	210.0	Alert, Nunavut, Canada
ZEP	78.90	11.88	475.0	Ny-Alesund, Svalbard (Spitsbergen), Norway and Sweden
SUM	72.58	-38.48	3238.0	Summit, Greenland
BRW	71.32	-156.60	11.0	Barrow, Alaska, USA
ICE	63.34	-20.29	127.0	Heimay, Vestmannaeyjar, Iceland
CBA	55.20	-162.72	25.0	Cold Bay, Alaska, USA
SHM	52.72	174.10	40.0	Shemya Island, Alaska, USA
UUM	44.45	111.10	914.0	Ulaan Uul, Mongolia
NWR	40.05	-105.58	3526.0	Niwot Ridge, Colorado, USA
AZR	38.77	-27.38	40.0	Terceira Island, Azores, Portugal
WLG	36.29	100.90	3810.0	Mt. Waliguan, People's Republic of China
BMW	32.27	-64.88	30.0	Tudor Hill, Bermuda, UK
IZO	28.30	-16.48	2360.0	Tenerife, Canary Islands, Spain
MID	28.21	-177.38	7.7	Sand Island, Midway, USA
ASK	23.18	5.42	2728.0	Assekrem, Algeria
MLO	19.53	-155.58	3397.0	Mauna Loa, Hawaii, USA
KUM	19.52	-154.82	3.0	Cape Kumukahi, Hawaii, USA
GMI	13.43	144.78	6.0	Mariana Islands, Guam
RPB	13.17	-59.43	45.0	Ragged Point, Barbados

CHR	1.70	-157.17	3.0	Christmas Island, Republic of Kiribati
SEY	-4.67	55.17	7.0	Mahe Island, Seychelles
ASC	-7.92	-14.42	54.0	Ascension Island, UK
SMO	-14.24	-170.57	42.0	Tutuila, American Samoa, USA
CGO	-40.68	144.68	94.0	Cape Grim, Tasmania, Australia
CRZ	-46.45	51.85	120.0	Crozet Island, France
TDF	-54.87	-68.48	20.0	Tierra Del Fuego, La Redonda Isla, Argentina
PSA	-64.92	-64.00	10.0	Palmer Station, Antarctica, USA
SYO	-69.00	39.58	14.0	Syowa Station, Antarctica, Japan
HBA	-75.58	-26.50	33.0	Halley Station, Antarctica, UK
SPO	-89.98	-24.80	2810.0	South Pole, Antarctica, USA

Table S2. NOAA aircraft profiles used for validation.

CODE	Location	Latitude (deg)	Longitude (deg)	Start Date	End Date
PFA	Poker Flat, Alaska, United States	65.07	-147.29	06/27/1999	06/05/2015
ESP	Estevan Point, British Columbia, Canada	49.6	-126.4	11/22/2002	06/09/2015
DND	Dahlen, North Dakota, USA	48.1	-98.0	09/21/2004	05/31/2015
LEF	Park Falls, Wisconsin, USA	45.9	-90.3	04/10/1998	05/28/2015
FWI	Fairchild, Wisconsin, USA	44.7	-91.0	09/20/2004	11/18/2005
NHA	Worcester, Massachusetts, USA	43.0	-70.6	09/21/2003	06/10/2015
BGI	Bradgate, Iowa, USA	42.8	-94.4	09/13/2004	11/18/2005
HFM	Harvard Forest, Massachusetts, USA	42.5	-72.2	11/11/1999	11/18/2007
WBI	West Branch, Iowa, USA	42.4	-91.8	09/14/2004	05/28/2015
OIL	Oglesby, Illinois, USA	41.3	-88.9	09/16/2004	11/19/2005
THD	Trinidad Head, California, USA	41.0	-124.2	09/02/2003	05/16/2015
BNE	Beaver Crossing, Nebraska, USA	40.8	-97.2	09/15/2004	05/11/2011
CAR	Briggsdale, Colorado, USA	40.6	-104.6	11/09/1992	04/21/2015
HIL	Homer, Illinois, USA	40.1	-87.9	09/16/2004	05/21/2015
TGC	Sinton, Texas, USA	27.7	-96.9	09/09/2003	06/05/2015
HAA	Molokai Island, Hawaii, USA	21.2	-158.9	05/31/1999	04/22/2008
RTA	Rarotonga, Cook Islands	-21.3	-159.8	04/16/2000	05/29/2015

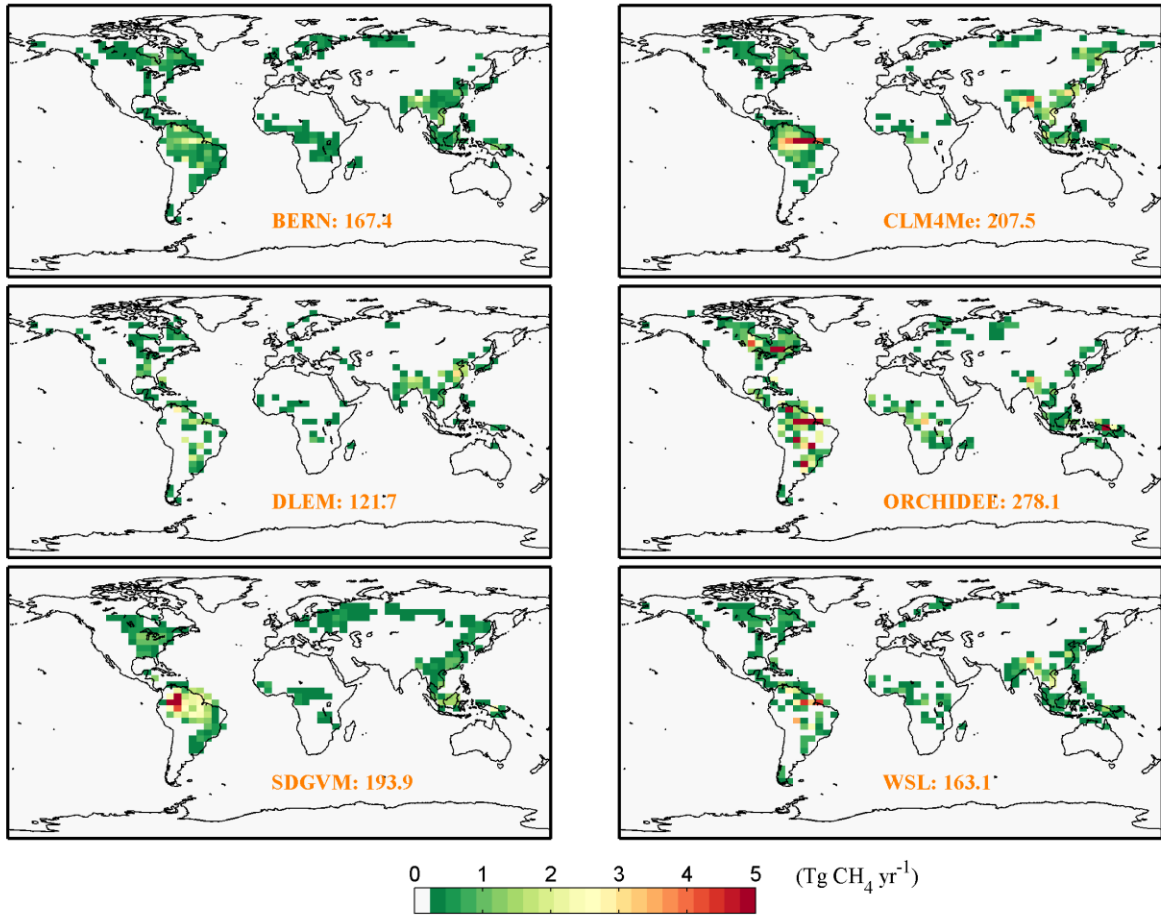


Figure S1. Average of prior wetland CH₄ annual emissions during 2004–2005 from six different wetland biogeochemical models used for the GEOS-Chem global inversion at 4° × 5° resolution. Annual total emission (orange) is presented in units of Tg CH₄ yr⁻¹.

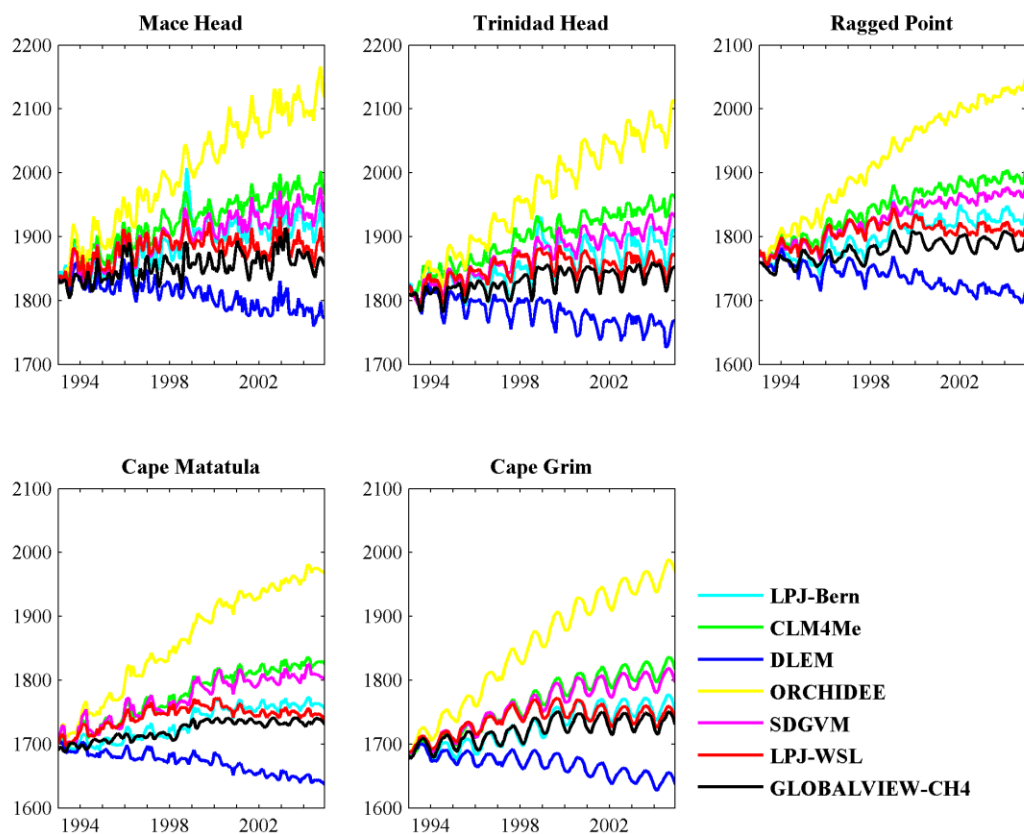


Figure S2. The comparison between the GEOS-Chem simulated and GLOBALVIEW-CH₄ atmospheric CH₄ (units: ppbv) at five stations (Mace Head, Ireland; Trinidad, California; Ragged Point, Barbados; Cape Matatula, Samoa; Cape Grim, Tasmania). The wetland CH₄ emissions used are pre-optimized model simulations provided by the WETCHIMP project.

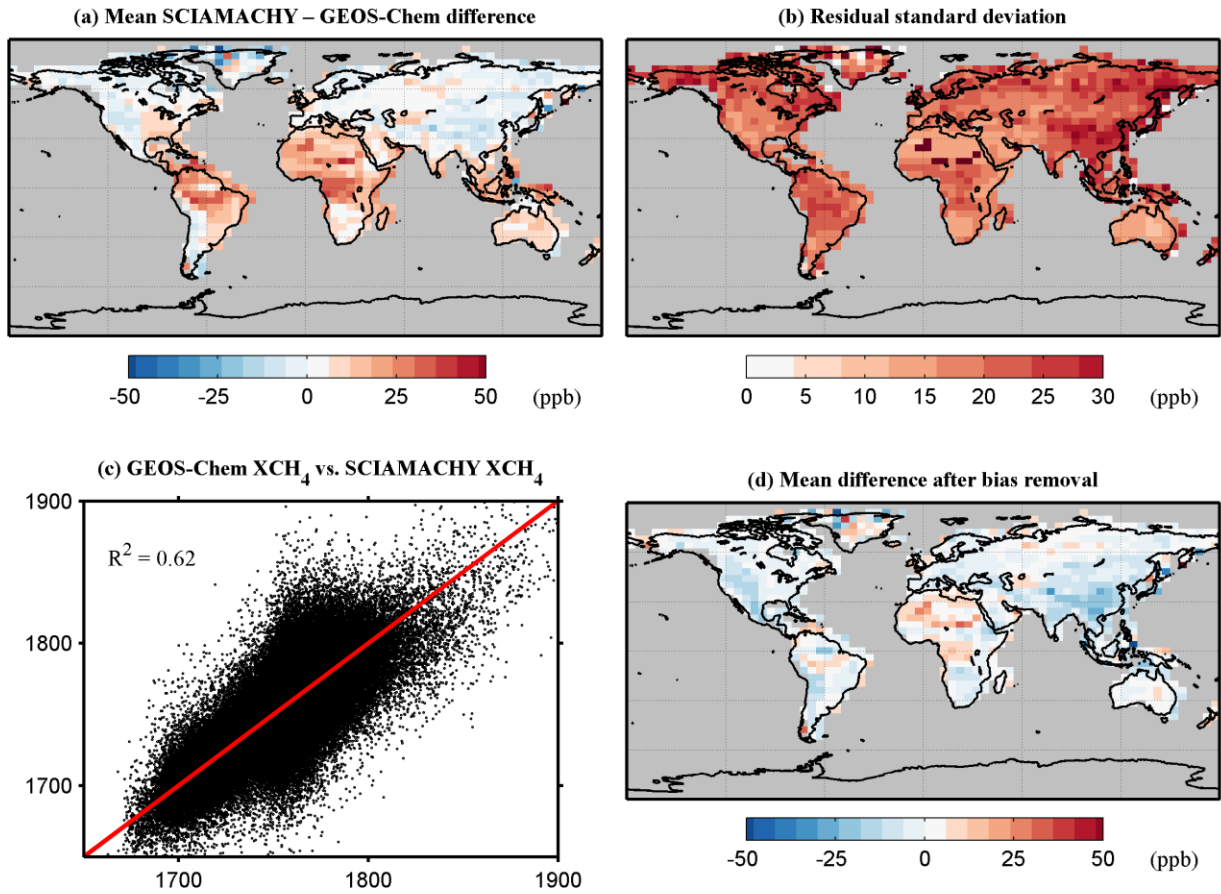


Figure S3. Comparison of column averaged CH_4 mole fractions from SCIAMACHY with those from GEOS-Chem model calculated with prior emissions. (a and b) show the mean bias and residual standard deviation of the satellite-model difference, (c) shows the comparison of the model (x axis) and satellite (y axis) XCH_4 after applying the “latitude + humidity” correction from the linear regression (weighted R^2 is shown inset and the red 1:1 line is also shown), and (d) shows the satellite-model difference after bias removal.

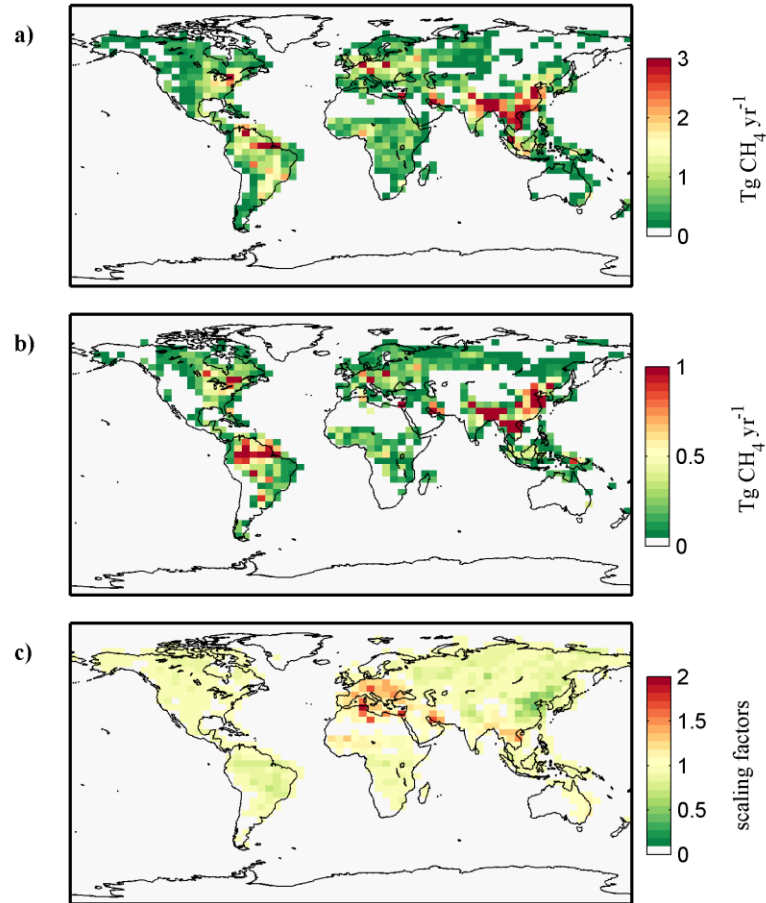


Figure S4. Optimized global CH₄ emissions and emission scale factors in 2005 at 4° × 5° resolution. Emission scale factor is defined as posterior emissions relative to prior emissions. a) Posterior CH₄ emissions averaged over inversions of six scenarios; b) standard deviation of posterior CH₄ emissions over inversions of six scenarios; c) optimized emission scale factors averaged over inversions of six scenarios.

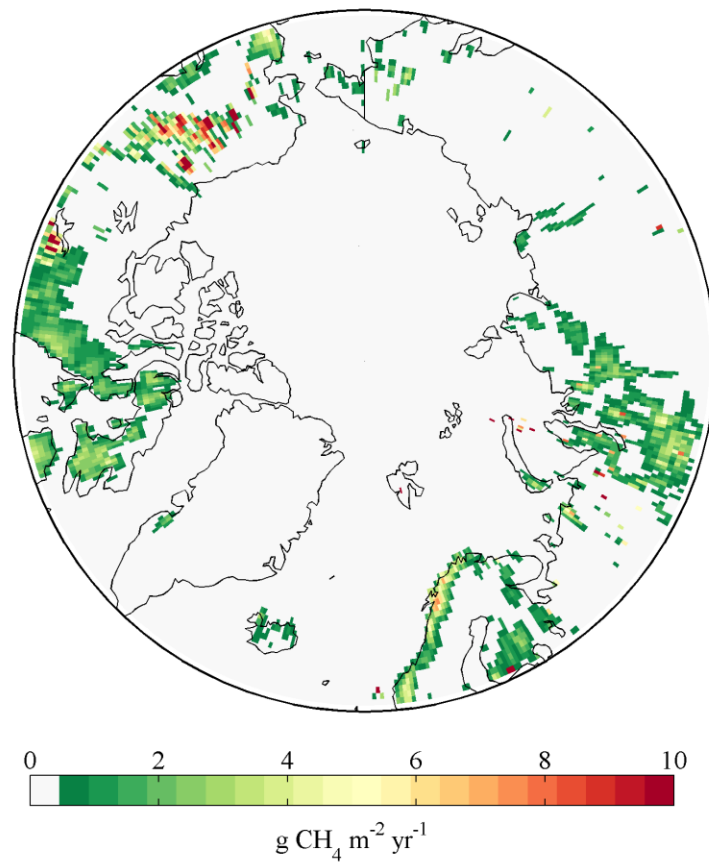


Figure S5. Posterior CH₄ emissions from the pan-Arctic in 2005 estimated by the inversion of the “DLEM wetland only” scenario. The “DLEM wetland only” scenario uses the simulated wetland CH₄ emissions from the DLEM model and does not incorporate CH₄ emissions from pan-Arctic lakes.

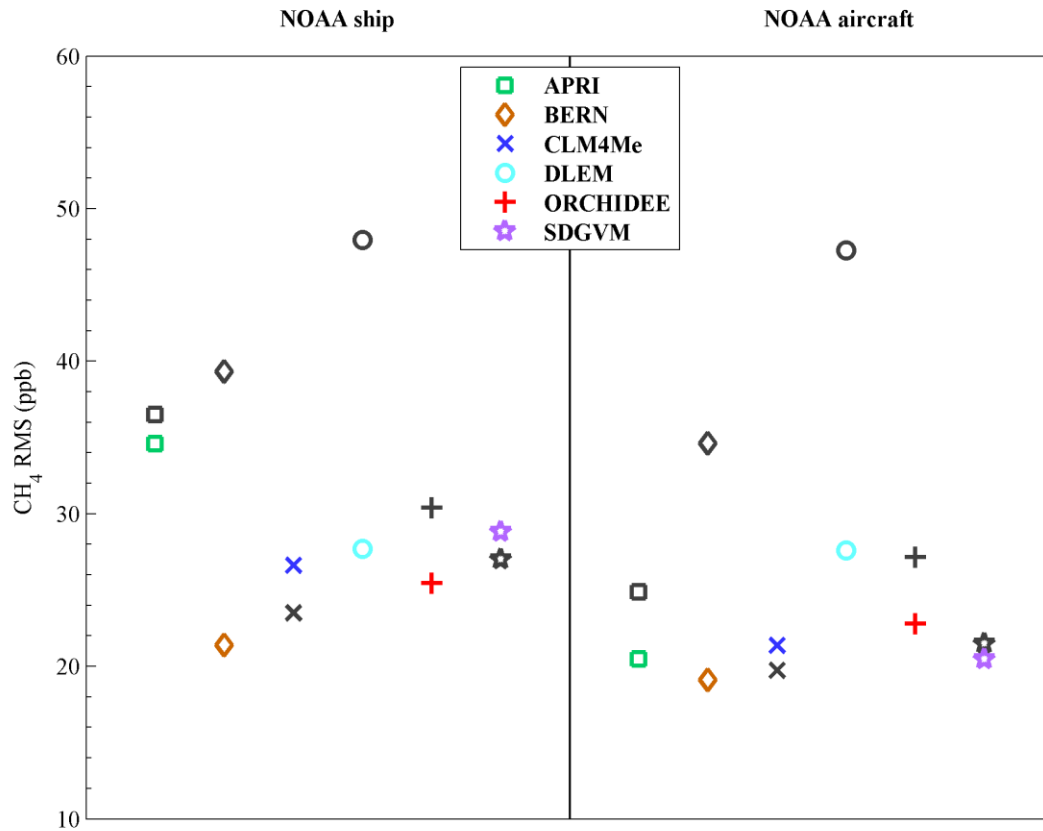


Figure S6. Evaluation of posterior GEOS-Chem CH₄ mole fractions from the global inversions with independent data sets. The plot shows the root mean square (rms) of differences between the modeled and the observed CH₄ mixing ratios. Black symbols indicate the rms of the forward GEOS-Chem runs.